Title

Warm Arctic, Cold Siberia Pattern: Role of Full Arctic Amplification Versus Sea Ice Loss Alone

Journal

Geophysical Research Letters, 47(17)

ISSN

0094-8276

Authors

Labe, Zachary
Peings, Yannick
Magnusdottir, Gudrun

Publication Date

2020-09-16

DOI

10.1029/2020gl088583

AGU ADVANCING EARTH AND SPACE SCIENCE

Geophysical Research Letters

RESEARCH LETTER
10.1029/2020GL088583

Warm Arctic, Cold Siberia Pattern: Role of Full Arctic Amplification Versus Sea Ice Loss Alone

Zachary Labe[1], **Yannick Peings**[1], **and Gudrun Magnusdottir**[1]

[1]Department of Earth System Science, University of California, Irvine, Irvine, CA, USA

Key Points:
- Climate models forced only by sea ice anomalies do not capture the vertical extent of Arctic warming during winter
- Increase in thickness of the winter 1,000–500 hPa layer is linked to a strengthening of the Siberian High and cold anomalies in eastern Asia
- Role of the stratosphere is unclear due to large internal variability at future global warming of 2° C above preindustrial levels

Supporting Information:
- Supporting Information S1

Correspondence to:
Z. Labe,
zlabe@uci.edu

Citation:
Labe, Z. M., Peings, Y., & Magnusdottir, G. (2020). Warm Arctic, cold Siberia pattern: Role of full Arctic amplification versus sea ice loss alone. *Geophysical Research Letters*, *47*, e2020GL088583. https://doi.org/10.1029/2020GL088583

Received 24 APR 2020
Accepted 4 AUG 2020
Accepted article online 10 AUG 2020

Abstract The effect of future Arctic amplification (AA) on the extratropical atmospheric circulation remains unclear in modeling studies. Using a collection of coordinated atmospheric and coupled global climate model perturbation experiments, we find an emergent relationship between the high-latitude 1,000–500 hPa thickness response and an enhancement of the Siberian High in winter. This wave number-1-like sea level pressure anomaly pattern is linked to an equatorward shift of the eddy-driven jet and a dynamical cooling response in eastern Asia. Additional simulations, where AA is imposed directly into the model domain by nudging, demonstrate how the sea ice forcing is insufficient by itself to capture the vertical extent of the warming and by extension the amplitude of the response in the Siberian High. This study demonstrates the importance of the vertical extent of the tropospheric warming over the polar cap in revealing the "warm Arctic, cold Siberia" anomaly pattern in future projections.

Plain Language Summary Surface air temperature averaged within the Arctic Circle is rising more than twice as fast as the rate of the globally averaged temperature. This is known as "Arctic amplification" and is the result of numerous feedbacks in the Earth system. This warming is not restricted to the surface, as the temperature is also increasing at least to the middle troposphere in the Arctic. The effects of this warming on weather patterns in the midlatitudes remain uncertain in observations and model simulations. In this study, we conduct a series of climate model experiments to better understand how the vertical extent of warming in the Arctic atmosphere connects to a strengthening of the Siberian High in boreal winter. This high-pressure response leads to colder air temperatures in eastern Asia through advection. We find that climate models prescribed with only Arctic sea ice loss do not fully capture the vertical extent of warming in the atmosphere, and thus underestimate the linkage between projected Arctic amplification and Eurasian climate.

1. Introduction

Assessing the response of the wintertime extratropical circulation to Arctic climate change remains unresolved in observations (Cohen et al., 2020) and future climate model projections (Smith et al., 2019). It is widely understood that the surface-albedo feedback, through loss of sea ice and snow cover, is only one of the important contributions to Arctic amplification (AA; Dai et al., 2019; Stuecker et al., 2018). Due to the nonlinear nature of polar feedbacks, it remains challenging to separate the relative importance of local and remote processes that result in AA (Goosse et al., 2018). While the largest AA has occurred near the surface in the zonal-mean average, there is evidence of substantial warming extending vertically into the upper troposphere in reanalysis and satellite-derived observations (Alexeev et al., 2012; Cohen et al., 2020; Graversen et al., 2008; Screen & Simmonds, 2011).

Recent work (e.g., Francis & Vavrus, 2015) has suggested that AA has led to a weakening of the midlatitude westerlies and an increase in the frequency of high-amplitude planetary wave regimes due to decreases in the latitudinal temperature gradient. Further, deep tropospheric warming may be important in resolving the mechanisms driving the "warm Arctic, cold Siberia" temperature anomaly pattern (He et al., 2020; Xu et al., 2019), and there is also evidence that the Arctic-midlatitude teleconnection is sensitive to the depth of vertical warming in idealized models (Sellevold et al., 2016). While it is currently not possible to attribute the continental cold extremes and atmospheric waviness to specific forcing due to the short observational record and substantial internal variability (Barnes & Screen, 2015; Blackport & Screen, 2020; Blackport et al., 2019; McCusker et al., 2016; Mori et al., 2019; Ogawa et al., 2018; Peings, 2019), a better understanding of

the effects of AA, not only sea ice loss, is still needed (Cohen et al., 2020). To address future climate linkages between the Arctic and midlatitudes, many studies have performed atmospheric general circulation model (AGCM) experiments by prescribing changes in the 21st century Arctic sea ice boundary conditions (e.g., Deser et al., 2010; Labe et al., 2018; Nakamura et al., 2016; Peings & Magnusdottir, 2014; Sun et al., 2015). However, most of these AGCM experiments have shown that warming is vertically trapped near the surface in response to sea ice forcing, which is unrealistic (Cohen et al., 2020). This may be due to a lack of ocean coupling (e.g., Blackport & Kushner, 2018; Deser et al., 2015), not allowing sea ice thickness (SIT) to change (Labe et al., 2018), and also to the fact that AA is in part driven by advection of heat and moisture from remote sea surface temperature (SST) changes (e.g., Perlwitz et al., 2015; Screen et al., 2012) and other climate feedbacks (Goosse et al., 2018; Park et al., 2018).

It remains an open question how important the vertical extent of the tropospheric warming is in assessing Arctic-midlatitude teleconnections (He et al., 2020). This also has implications for improving our understanding of the intermodel spread of the eddy-driven jet response in the latest Coupled Model Intercomparison Project (CMIP) projections due to the competing "tug-of-war" effects between upper troposphere tropical warming and AA (Barnes & Polvani, 2015; Peings et al., 2018, 2019; Vavrus, 2018; Zappa et al., 2018); although the amplification of tropical warming remains uncertain in model simulations (Santer et al., 2017). To answer this question, we make use of a collection of large ensemble experiments that are prescribed with different levels of sea ice forcing and AA. Here we focus our attention on understanding the tropospheric pathway by which sea ice anomalies modulate the Northern Annular Mode (NAM; Thompson & Wallace, 1998) through eddy-mean flow interactions and the excitation of Rossby waves, which can reinforce anticyclonic anomalies over Eurasia (Honda et al., 2009; Nakamura et al., 2016). By doing so, we find an emergent relationship between anomalies of the geopotential thickness of 1,000–500 hPa thickness layer over the Arctic and the response of the Siberian High. We also examine the degree of linearity in the responses to different levels of AA forcing in the GCM by nudging the temperature directly in the Arctic and maintaining the thermal anomaly throughout the simulation. The results have implications for disentangling the sensitivity of the large-scale atmospheric response to varying amounts of projected Arctic sea ice decline from that associated with deep-tropospheric AA.

2. Climate Model Experiments and Analysis

We primarily use two sets of experiments to understand the role of different levels of projected warming in the Arctic mid-troposphere on Arctic-midlatitude teleconnections: (1) a set of simulations forced by future sea ice loss only and (2) a set of simulations where the projected total warming (full AA effect), taken from a fully coupled global climate model, is prescribed. Table 1 contains a complete list of individual experiments, and Figure S1 in the supporting information compares their different levels of sea ice forcing equivalents.

The AGCM numerical experiments are implemented using the National Center for Atmospheric Research (NCAR) Whole Atmosphere Community Climate Model, version 4 (WACCM; Marsh et al., 2013) and the Department of Energy (DOE) Energy Exascale Earth System Model, version 1 (E3SM; Golaz et al., 2019). WACCM includes 66 vertical levels (5.1×10^{-6} hPa, ~140 km) and uses CAM4 physics. We use the specified chemistry version of WACCM (Smith et al., 2014), which is cheaper in computational cost, but simulates dynamical coupling and stratospheric variability that is comparable to the interactive chemistry model version. The WACCM experiments are run with a horizontal resolution of 1.9° latitude by 2.5° longitude and include year 2000 radiative forcings. A repeating 28-month cycle of the quasi-biennial oscillation (QBO) is included in the WACCM experiments by using a nudging technique to relax the equatorial stratospheric winds to observed radiosonde data.

The E3SM atmospheric component was developed from CAM5.3 and includes additional turbulence parameterizations and improvements to cloud and aerosol physics (Rasch et al., 2019). E3SM includes 72 vertical layers (compared to 30 in CAM5) with a model top at ~0.1 hPa (~60 km). We use the lower-resolution version of E3SM with a horizontal resolution of 1° and year 2000 radiative forcings. While the model includes an internally generated QBO-like oscillation of the equatorial stratospheric wind, the period is too short, and the westerly winds are too strong (Richter et al., 2019).

Table 1
List of Climate Model Experiments Used in This Study

Experiment	Model protocol	Forcing				$\Delta\bar{T}_{1,000-500}$
		SST	SIC	SIT	AA	
ΔAMIP	Transient; 1979–2016	X	X			+0.72
ΔE3SM-SIC-Pd	AGCM; Present day		X			+0.76
ΔWACCM-SIC-Pd	AGCM; Present day		X			+0.80
ΔAA-2030	**AGCM; $\overline{2020-2039}$**				**X**	**+0.86**
ΔS-Coupled-Pd	Coupled; Present day		X			+0.93
ΔWACCM-SIT-Pd	AGCM; Present day		X	X		+0.99
ΔAMIP-HL	**Transient; 1979–2016**	**X**	**X**		**X**	**+1.10**
ΔE3SM-SIC-Pi	AGCM; Preindustrial		X			+1.22
ΔWACCM-SIC-Pi	AGCM; Preindustrial		X			+1.40
ΔS-Coupled-Pi	Coupled; Preindustrial		X			+1.59
ΔNET	AGCM; $\overline{2051-2080}$		X	X		+1.86
ΔAA-2060	**AGCM; $\overline{2050-2069}$**				**X**	**+2.94**
ΔAA-2090	**AGCM; $\overline{2080-2099}$**				**X**	**+4.84**

Note. Experiments with AA forcing are highlighted with bold text. The overbar indicates a time mean for the forcing level. Different combinations of forcing (SST variability, SIC, SIT, and AA nudging) are marked for each experiment. For the boundary forced experiments (not in bold), we compare 2°C warming equivalent forced experiments to conditions in the Model Protocol column. The ensemble mean December-January-February (DJF) 1,000–500 hPa air temperature response ($\Delta\bar{T}_{1,000-500}$; °C) can be found in the fourth primary column for each experiment. The $\Delta\bar{T}_{1,000-500}$ anomalies are area/pressure-weighted averages calculated over the polar cap (north of 65°N latitude). The experiments are sorted in ascending order by their $\Delta\bar{T}_{1,000-500}$ response.

2.1. Atmosphere-Only Simulations

2.1.1. Role of Future Arctic Sea Ice

The first set of AGCM experiments is conducted following the Polar Amplification Model Intercomparison Project (PAMIP; Smith et al., 2019) Tier 1 protocol. It consists of 100 members of 14-month (April through May of the following year) simulations with prescribed SST and sea ice concentration (SIC) representative of future conditions that are compared to two different control runs corresponding to preindustrial (Pi) and present-day (Pd) boundary forcing. Future sea ice fields are constructed from an ensemble of 31 CMIP5 models (Representative Concentration Pathway 8.5) representing 2°C of global warming above preindustrial level (Figure S1). The Pd simulation is conducted using average SST and SIC from a 1979–2008 annual cycle climatology in HadISST1 (Rayner et al., 2003). The Pi SIC is derived from Pi control runs of the same 31 CMIP5 models for 30-year periods representing a global mean temperature of 13.67°C (see details on the PAMIP forcing fields in Smith et al., 2019). SSTs are held to Pd values, except in grid cells where SIC differs by more than 10% compared to Pi/future experiments (Peings & Magnusdottir, 2014; Screen et al., 2013). SIT is held constant throughout the Arctic at 2 m. To isolate the effect of SIC in each model, we take the difference of the future experiment minus Pd (denoted as ΔWACCM-SIC-Pd or ΔE3SM-SIC-Pd) and Pi (denoted as ΔWACCM-SIC-Pi or ΔE3SM-SIC-Pi).

An additional set of experiments using WACCM is conducted to include the effects of SIT decline between future and Pd conditions (denoted at ΔWACCM-SIT-Pd). For fields of SIT, Pd conditions are taken from the Pan-Arctic Ice Ocean Modeling and Assimilation System, version 2.1 (PIOMAS; Schweiger et al., 2011), and future conditions are taken from the ensemble of the 31 CMIP5 models. SST and SIC fields follow the same protocol as previously described for ΔWACCM-SIC-Pd.

Finally, we compare the above PAMIP experiments, which consider future warming conditions of 2°C that occurs around the mid-21st century, to an experiment with a stronger sea ice forcing (denoted as ΔNET). This WACCM experiment isolates the role of sea ice loss in the late 21st century (2051–2080 minus 1976–2005) using forcing fields from the mean of 40 ensemble members in the Community Earth System Model Large Ensemble (LENS; Kay et al., 2015). More details about this experiment can be found in Labe et al. (2018, 2019).

2.1.2. Role of AA

To quantify the effect of sea ice-only forcing in AA, we use three experiments of WACCM where AA is directly imposed in the model domain by nudging -corresponding to the projected state of the Arctic in 2030, 2060, and 2090 (Peings et al., 2019). A 51-year control simulation is conducted using a repeating cycle of SST and SIC taken from the 1979–2008 climatology in HadISST1. To assess the influence of AA, three perturbation experiments are conducted using a regional nudging within the Arctic (>70°N) in the lower troposphere (from the surface to 600 hPa) to temperature fields representing conditions in the early (2020–2039), middle (2050–2069), and late (2080–2099) 21st century within the mean of 40 ensemble members from LENS. This projected warming includes the direct influence from external forcings as well as any model feedbacks in LENS. Fields of SST and SIC follow the same repeating cycle as the control simulation (Figure S1). To isolate the effect of AA, we take the difference between the perturbation experiments and the control (denoted as ΔAA-2030, ΔAA-2060, and ΔAA-2090). Details and validation of the nudging protocol can be found in Peings et al. (2019).

2.2. Atmosphere-Only Transient Simulations

To compare our WACCM simulations with observations, we utilize two transient AGCM experiments with 10 ensemble members each. The first simulation follows the standard Atmospheric Model Intercomparison Project II protocol (AMIP; Taylor et al., 2000) with monthly SST and SIC variability over the 1979 to 2016 period. SIT is prescribed to 2 m. This experiment is denoted as ΔAMIP. In a second transient simulation (denoted as ΔAMIP-HL), we follow the same setup as ΔAMIP, but instead apply a nudging scheme (as in section 2.1.2) to the Arctic Circle (>65°N) troposphere (up to 300 hPa). In that domain, temperature, horizontal winds, and surface pressure are nudged toward observed 3-hr anomalies, superimposed on the model 3-hr climatology. Thus, we prescribe the observed variability of the atmosphere in high latitudes while retaining the model mean state. The 3-hr observed anomalies are from the NASA's Modern-Era Retrospective Analysis for Research and Applications, version 2 (MERRA2; Gelaro et al., 2017). We compare ΔAMIP and ΔAMIP-HL to monthly observations from the National Centers for Environmental Prediction/NCAR reanalysis project (NCEP/NCAR R1; Kalnay et al., 1996) and the European Centre for Medium-Range Weather Forecasts (ECMWF) next-generation reanalysis ERA5 (Hersbach et al., 2020).

2.3. Coupled Atmosphere-Ocean Simulations

We consider a set of coupled experiments to compare the short-term (S) effects of ocean coupling on the atmospheric response to Arctic sea ice loss. In this experiment (denoted as ΔS-Coupled-Pi or ΔS-Coupled-Pd), each WACCM ensemble member is run for 14 consecutive months (April through May of the following year) with an interactive ocean and follows the same PAMIP forcing for Pi, Pd, and future sea ice conditions. To have similar sea ice fields as in the AGCM simulations (see section 2.1.1), SIT is nudged to its prescribed value in the AGCM runs, that is, 2 m.

2.4. Statistical Testing

Here we focus our analysis on the boreal winter (DJF; December-January-February) when the ensemble mean atmospheric response to Arctic sea ice decline is found to be the largest (e.g., Blackport & Screen, 2019; Deser et al., 2010). We use a two-sided Student's *t* test and control for field significance using the false discovery rate (FDR; Wilks, 2016). A response is considered statistically significant if the FDR-adjusted *p* value is less than 0.05, unless otherwise stated.

3. Results

Figure 1 shows the DJF near-surface (2 m) air temperature response in the AA (a–c) and Pd sea ice-forcing PAMIP experiments (d–f). There is a nearly uniform warming over the Arctic Ocean in response to the AA forcing (Figures 1a–1c). The ΔAA-2090 warm anomalies range from more than 10°C over the central Arctic to only 1–3°C over parts of North America, as far south as around 45°N latitude (Figure 1c). Thus, even under the late 21st century AA forcing, the thermodynamic warming remains mostly confined to the polar cap. However, a cooling response (down to ∼−2°C) is revealed in eastern Asia in ΔAA-2060. This cooling is amplified in ΔAA-2090 with negative temperature anomalies (down to ∼−4°C) expanding westward across Siberia.

Similar to ΔAA-2060, the warming response to sea ice loss in the short-coupled experiment (ΔS-Coupled-Pd) is uniform across the Arctic Ocean (Figure 1e). Without ocean coupling, the near-surface temperature

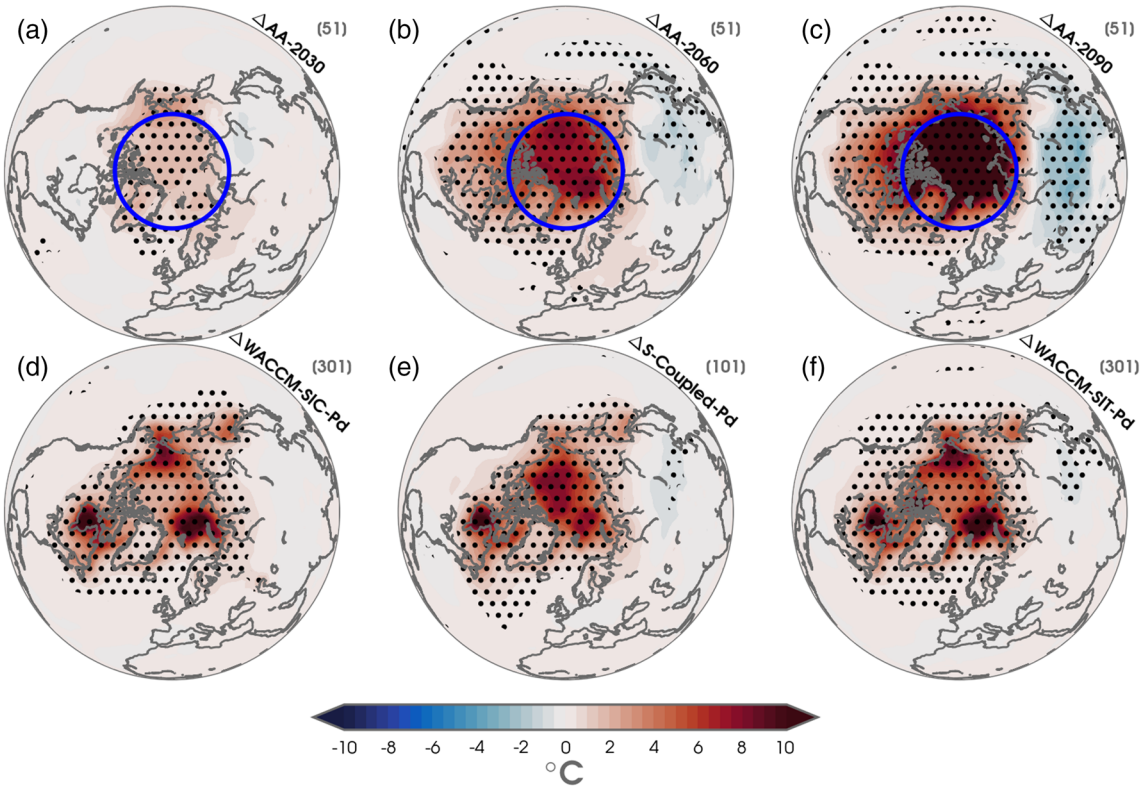

Figure 1. (a) Boreal winter (December-February) 2-m air temperature anomalies (interval of 0.5°C) for ΔAA-2030. (b) Same as (a) but for ΔAA-2060. (c) Same as (a) but for ΔAA-2090. (d) Same as (a) but for ΔWACCM-SIC-Pd. (e) Same as (a) but for ΔS-Coupled-Pd. (f) Same as (a) but for ΔWACCM-SIT-Pd. Statistically significant anomalies are overlaid with black stippling at the 95% confidence level after adjusting for FDR. The number of ensemble members for each experiment is listed in the upper right-hand corner in gray. The blue circle marks the boundary of the nudging domain (poleward of 70°N) in (a)–(c).

response is greatest in the outer marginal seas (e.g., Barents-Kara Seas) in direct association with the sea ice forcing (Figures 1d and 1f). This suggests that even on short time scales, ocean feedbacks may contribute to further high-latitude warming in the Arctic (e.g., north of 75°N latitude). However, this is not the case with the land temperature response, which is meridionally confined to the Arctic within the PAMIP experiments (Figures 1d–1f). Again, we find a small patch of cooling over eastern Asia in the ΔS-Coupled-Pd and ΔWACCM-SIT-Pd experiments. This "warm-Arctic, cold Siberia" pattern is in agreement with earlier studies (e.g., Labe et al., 2018; Mori et al., 2014, 2019; Nakamura et al., 2015; Peings & Magnusdottir, 2014) and can be linked to a strengthening of the Siberian High (Labe et al., 2019; Screen et al., 2015; Sun et al., 2015). The dynamically induced cooling results from cold air advection in association with a strengthening of the Siberian High. This is consistent with northerly meridional wind anomalies found near the surface over Eurasia in our experiments (not shown). Overall, despite differences in magnitude, we find strikingly similar patterns of temperature response in WACCM in the sea ice-forcing (coupled/uncoupled) and AA experiments.

As with the 2-m air temperature response, the sea level pressure (SLP) response in the ΔAA-2030 experiment is weak and statistically insignificant (Figure 2a). However, a different picture emerges with stronger AA forcing. The response in ΔAA-2060 (Figure 2b) is robust and characterized by higher SLP anomalies stretching from Greenland to Eurasia and lower SLP anomalies over the central Arctic Ocean and in the vicinity of the Aleutian Low. This dipole pattern of SLP anomalies resembles a zonal wave number-1-like pattern and is further amplified in ΔAA-2090 (Figure 2c). The circulation response exhibits an equivalent barotropic structure over the North Pacific and North Atlantic. However, the response is baroclinic over the Arctic Ocean with positive anomalies of geopotential heights at 500 hPa (Z500) resembling a negative phase of the NAM (Figure S2). The pattern of SLP anomalies in ΔAA-2060 and ΔAA-2090 is also quite similar to that of ΔNET (Figure 2c in Labe et al., 2018). The response to increasing levels of AA forcing reinforces the wave-1 SLP pattern and suggests that the large-scale circulation response may be linear.

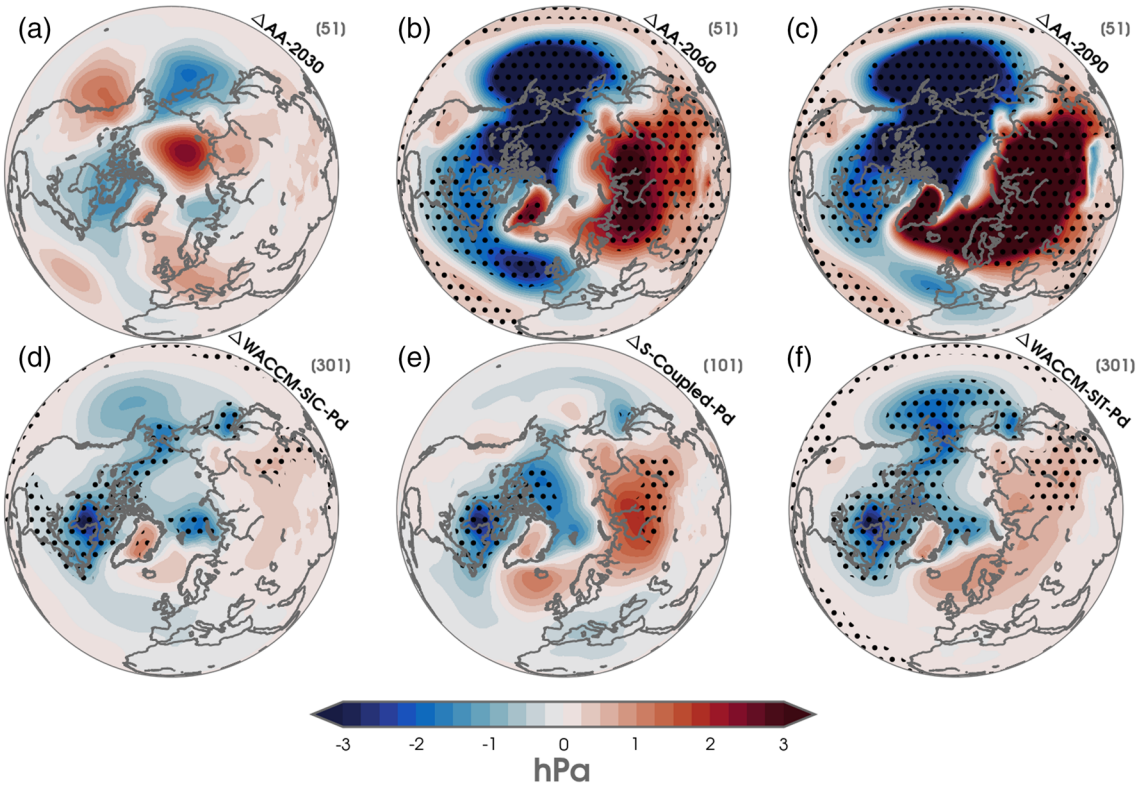

Figure 2. Same as Figure 1, but for the mean sea-level pressure response (interval of 0.25 hPa) in each experiment.

In contrast to ΔAA-2060 and ΔAA-2090, we find a smaller SLP response to the Pd sea ice forcing in the three PAMIP experiments (Figures 2d–2f). Decreases in SLP are found in the vicinity of the SIC anomalies (cf. Figure 5f in Smith et al., 2019) and over the Hudson Bay. We also find an increase in SLP over Eurasia, albeit weaker than ΔAA-2060. The spatial extent of SLP anomalies is largest in the combined SIC and SIT-forcing experiment (ΔWACCM-SIT-Pd). The robustness of this stronger response was tested by adding additional ensemble members for a total ensemble size of 300 (compared to the recommended 100 in PAMIP protocol). This result is in agreement with Labe et al. (2018) indicating that loss of SIT reinforces the large-scale atmospheric response to SIC anomalies (Figure 2d). Although there are substantial differences in magnitude, the pattern of the wintertime SLP response in the coupled (Figure 2e) and uncoupled sea ice-forcing experiments (Figures 2d and 2f) still resembles the wave-1 response found in ΔAA-2060 and ΔAA-2090.

We now turn to vertical cross sections of the zonal-mean temperature response to better understand the differences in magnitude of the surface response. Figure 3 shows the zonal-mean temperature response as a function of height (pressure) for each of the experiments. Statistically significant warming extends up to 500 hPa in ΔAA-2060 (Figure 3b) and up to 300 hPa in ΔAA-2090 (Figure 3c). Recall that the nudging only extends to 600 hPa. In contrast, vertical warming is much smaller and confined to the lower troposphere within the sea ice-forcing experiments (Figures 3d–3f). Warming reaches up to 500 hPa due to both SIT and SIC loss (ΔWACCM-SIT-Pd), but only up to about 700 hPa in the SIC-only forced experiment (ΔWACCM-SIC-Pd).

To contrast this simulated vertical warming with recent observations, we compare cross sections of the zonal-mean temperature difference in the most recent decade (2019–2010) minus the first decade of the satellite era record (1988–1979) in Figure S3. The last decade (2019–2010) overlaps with an observed period of substantial AA (Cohen et al., 2020). There is close agreement in the structure of vertical warming between ERA5 and NCEP/NCAR R1 data sets with statistically significant warming extending up to 300 hPa above portions of the Arctic. The largest warming is found in the lower troposphere (up to 850 hPa) and poleward of 75°N latitude. While we cannot rule out internal variability, this suggests that the sea ice-only forcing experiments do not capture key processes that are important for AA in the middle-to-upper troposphere (Francis, 2017; Perlwitz et al., 2015).

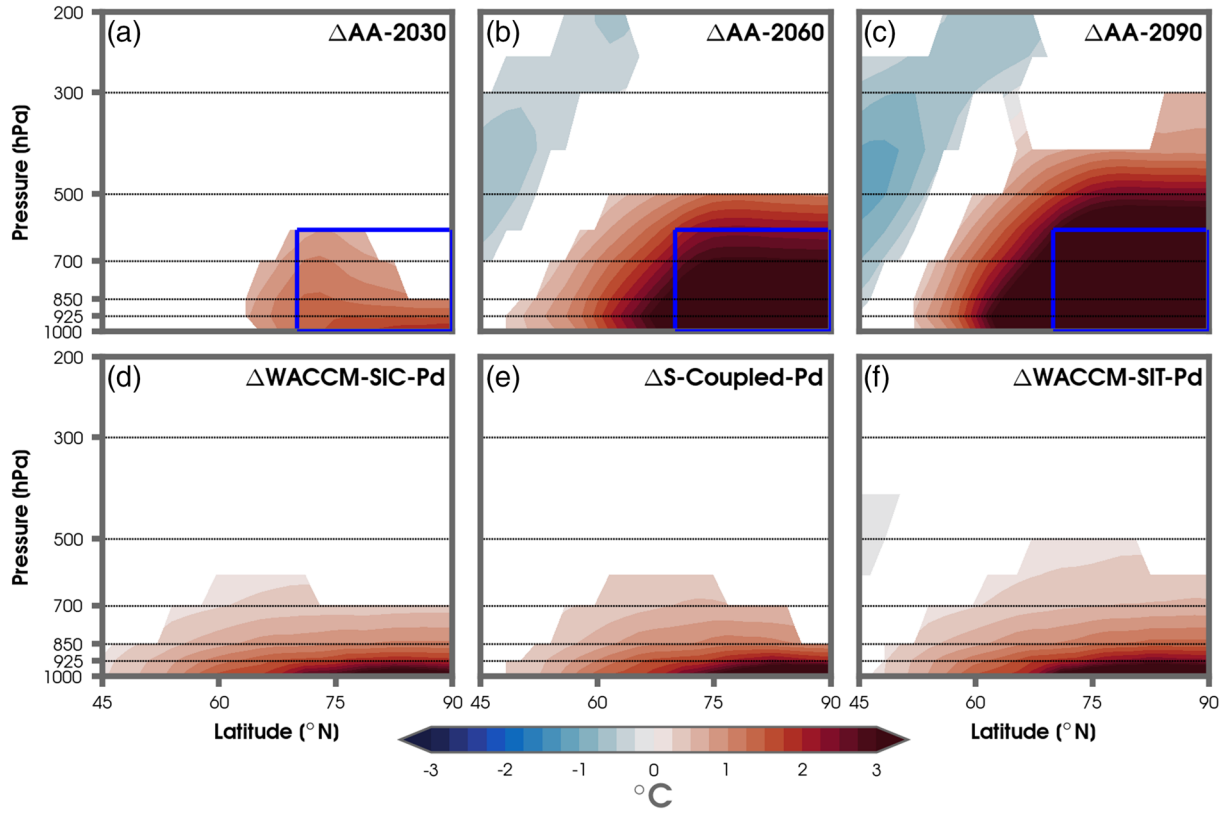

Figure 3. (a) Average December-February zonal-mean air temperature anomalies (interval of 0.25°C) as a function of height (pressure) for ΔAA-2030. (b) Same as (a) but for ΔAA-2060. (c) Same as (a) but for ΔAA-2090. (d) Same as (a) but for ΔWACCM-SIC-Pd. (e) Same as (a) but for ΔS-Coupled-Pd. (f) Same as (a) but for ΔWACCM-SIT-Pd. Shading is only shown for statistically significant responses after controlling for FDR at the 95% confidence level. The blue box outlines the nudging domain for the AA experiments (a–c).

Figure S4 shows the response of the 1,000–500 hPa thickness for the AA and PAMIP experiments. As expected, the largest tropospheric thickness increases (>40 m) are found in simulations with the highest vertical extent of warming in Figure 3. This reveals a uniform increase in thickness over the Arctic Ocean in ΔAA-2060 (Figure S4b) and ΔAA-2090 (Figure S4c) due to AA forcing. We also find a decrease in thickness extending from the North Pacific to Siberia in association with troughing and surface cooling downstream of the Siberian High. The spatial pattern of tropospheric thickness anomalies is consistent in the sea ice-forcing experiments, although the change is smaller in magnitude (Figures S4d–S4f). The largest increases in thickness are found over the Hudson Bay and the Barents-Kara Seas. Moreover, the only statistically significant decrease in thickness is found in ΔWACCM-SIT-Pd over Siberia (Figure S4f).

To evaluate the dynamical effect of a reduction in the meridional tropospheric thickness gradient, we plot the monthly mean response of the eddy-driven jet in Figure S5. In all experiments, we find a weakening on the poleward flank of the eddy-driven jet from October through March. However, this weakening of the 700-hPa zonal wind (U700) is only statistically significant in the ΔAA-2060 (Figure S5b), ΔAA-2090 (Figure S5c), and ΔWACCM-SIT-Pd (Figure S5f) experiments and is largest over eastern Siberia (not shown). In addition to the weakening, there is an equatorward shift of the eddy-driven jet with positive anomalies of U700 around 40°N latitude, especially in ΔAA-2060 and ΔAA-2090. The positive anomalies of U700 are mostly insignificant in the ΔWACCM-SIT-Pd experiment. Note that there are again similarities in the pattern of U700 anomalies between experiments despite the differences in forcing, number of ensemble members, and model setup.

Some studies have pointed to the role of the stratosphere in linking the Siberian cooling pattern to Arctic sea ice anomalies (e.g., Cohen et al., 2020; Kim et al., 2014; Labe et al., 2019; Peings & Magnusdottir, 2014; Sun et al., 2015; Zhang et al., 2018). However, we do not find that to be the case for the PAMIP experiments in response to the relatively small sea ice-forcing at 2°C of future climate warming. Figure S6 shows the

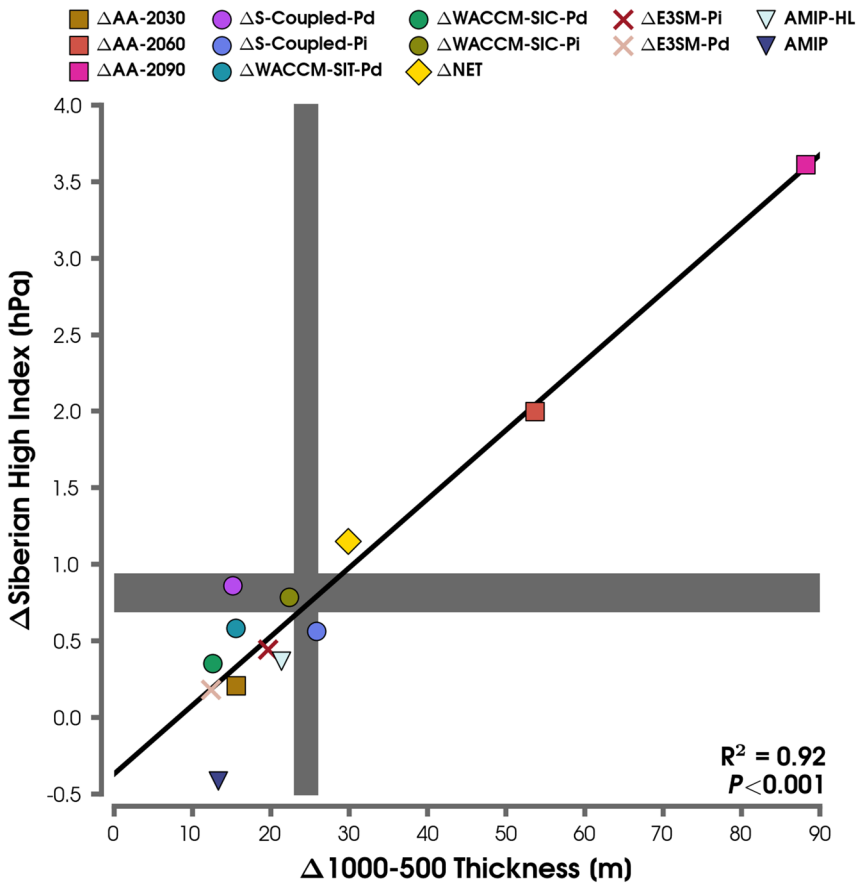

Figure 4. Dependence of the Siberian High Index on the 1,000–500 hPa layer thickness response averaged over the polar cap (>65°N) for the boreal winter (December-February). The AA nudging experiments are marked using squares. Responses for the coupled and uncoupled sea ice experiments in WACCM are shown with circular points for PAMIP and using a diamond for ΔNET. The responses in the AMIP-style (WACCM) simulations are shown with downward triangles. The responses in E3SM are indicated by X marks. Gray shading indicates the range in 1,000–500 hPa layer thickness anomalies (vertical bar; 2019–2010 minus 1988–1979) and for the Siberian High Index (horizontal bar; 2019–2010 minus 1988–1979) between ERA5 and NCEP/NCAR R1. The black line shows the linear (least squares) fit after taking into consideration all of the climate model experiments.

geopotential height response at 50 hPa (Z50) for the AA and sea ice-forcing experiments. We do not find a significant change in the stratospheric mean state at Z50 for the sea ice experiments (Figure S6d–S6f) nor for ΔAA-2030 (Figure S6a). However, in response to greater AA, we do find an increase in Z50 heights over the polar cap in association with a warming of the stratospheric polar vortex. This weakening of the polar vortex may be linked to the greater equatorward shift of the eddy-driven jet found in Figure S5b–S5c (Peings et al., 2019).

We refine our understanding of the wintertime relationship between the vertical warming of the mid-troposphere and the response of the Siberian High by using an emergent constraints-like approach (e.g., Hall et al., 2019) in Figure 4. In this assessment, we consider additional coupled and uncoupled WACCM experiments along with AGCM simulations using E3SM. Further, we use two transient atmosphere-only experiments (ΔAMIP and ΔAMIP-HL) by considering the difference in their first and last 10-year epochs (2016–2007 minus 1988–1979). We find a highly positive linear correlation ($R^2 = 0.92$; $p < 0.001$) between the response of the 1,000–500 hPa thickness layer over the polar cap (weighted average north of 65°N latitude) and the Siberian High Index (weighted average over 40–65°N and 80–120°E; Panagiotopoulos et al., 2005) after considering all of the experiments irrespective of forcing, model, or model setup (black line). Lastly, we compare this modeled linear relationship with 10-year epoch differences (2019–2010 minus 1988–1979) in reanalysis data using gray shading to represent the range between ERA5 and NCEP/NCAR R1 (Figure 4). While these 10-year epochs are too short to make attribution statements on a forced response, due to decadal

and multidecadal internal variability, they add confidence to the interpretation of this Siberian High relationship with increases in tropospheric thickness over the polar cap. Unsurprisingly, with a larger sea ice-forcing (Pi compared to Pd), we find more warming and a stronger response of the Siberian High (ΔWACCM-SIC-Pi and ΔE3SM-SIC-Pi).

Since ΔNET is forced with late 21st century SIC and SIT boundary conditions from LENS using WACCM (Labe et al., 2018, 2019), we can compare this experiment with the nudging experiments that reflect the total large-scale atmospheric response to AA. We find that both the mid-tropospheric warming and Siberian High responses are much smaller in ΔNET (see also Table 1). This further illustrates the importance of the other feedbacks contributing to vertical warming in the Arctic, rather than only surface forcing from sea ice boundary conditions.

We note that ΔAMIP is an outlier relative to the other experiments. However, we can compare ΔAMIP to ΔAMIP-HL, which nudges the high latitudes to observed tropospheric air temperatures (up to 300 hPa). ΔAMIP-HL is warmer in the lower-to-middle troposphere and is in closer agreement to the reanalysis data sets (gray shading) and modeled linear relationship (black line) in Figure 4. This supports earlier studies (e.g., Perlwitz et al., 2015) that the ensemble mean response in AMIP-style experiments, with observed SST and SIC variability, does not capture the total AA effect found in recent reanalysis, especially in the midtroposphere.

4. Conclusions

In summary, we use an extensive number of large ensemble perturbation experiments with different combinations of AA (total atmospheric thermal response to external forcings and feedbacks) and sea ice-only forcing to understand the relationship between Arctic warming and Siberian cooling in boreal winter. We find that the vertical extent of warming into the middle troposphere over the Arctic is important for revealing this surface temperature anomaly pattern. Using an integrated approach, we find that an increase in the 1,000–500 hPa thickness layer over the polar cap is associated with a strengthening of the Siberian High. The emergence of a zonal wave number-1 SLP anomaly pattern and weakening on the poleward flank of the eddy-driven jet are also closely linked to the magnitude of warming in the middle troposphere. Using a novel set of nudging experiments, we also show that this SLP pattern is reinforced with increasing levels of future AA. Moreover, the cooling response over Eurasia is also enhanced with greater AA (not considering other greenhouse gas forcing) and occurs downstream of the Siberian High anomaly due to cold air advection. Warming is vertically trapped near the surface in experiments prescribed only with changes in Arctic sea ice, and increasing sea ice loss is not enough to get the full extent of the influence of AA in the midlatitudes. The strength of the Siberian cooling cannot be explained by a response to sea ice change alone, but actually depends on the full range of external forcing and coupled feedbacks on the Arctic tropospheric temperatures. Overall, the dynamical response to the PAMIP sea ice forcing at 2°C is small and nonrobust relative to internal variability when compared with present-day conditions. This low signal-to-noise ratio will be the subject of future work.

Our results are consistent with Xu et al. (2019) and He et al. (2020), who found that the vertical extent of warming over the Barents-Kara Seas can help resolve differences in the strength of Arctic-midlatitude linkages in historical simulations. While we primarily make use of one model (WACCM), we find that atmospheric thickness is also closely coupled to the Siberian High response in E3SM (Figure 4). Our results, in conjunction with He et al. (2020), contribute further evidence to the importance of understanding how realistically CMIP6 models simulate the vertical structure of future Arctic warming, and thus the strength of Arctic midlatitude linkages in wintertime.

Data Availability Statements

Sea ice fields from LENS are publicly available at this site (https://www.cesm.ucar.edu/projects/community-projects/LENS/data-sets.html). Model data from the AA nudging experiments are available on Zenodo (https://zenodo.org/record/3066448 and https://zenodo.org/record/3903536). PAMIP experiment data are publicly available at this site (https://www.earthsystemgrid.org/). Monthly reanalysis data are publicly available for NCEP/NCAR R1 (https://www.esrl.noaa.gov/psd/data/gridded/data.ncep.reanalysis.html), MERRA2 (https://gmao.gsfc.nasa.gov/reanalysis/MERRA-2/), and ERA5 (https://climate.copernicus.eu/climate-reanalysis).

Acknowledgments
We thank two anonymous reviewers and the Editor for their constructive comments to improve this study. This project was supported by DOE Grant DE-SC0019407 and NSF Grant AGS-1624038. We also acknowledge high-performance computing support for SC-WACCM4 from Cheyenne (doi: 10.5065/D6RX99HX) provided by NCAR's Computational and Information Systems Laboratory, sponsored by the National Science Foundation. E3SM simulations were performed using resources from National Energy Research Scientific Computing Center, a U.S. Department of Energy Office of Science User Facility. Figures were generated using Python 3.7, Matplotlib 3.1, and colormaps provided by Thyng et al. (2016).

References

Alexeev, V. A., Esau, I., Polyakov, I. V., Byam, S. J., & Sorokina, S. (2012). Vertical structure of recent Arctic warming from observed data and reanalysis products. *Climatic Change*, *111*(2), 215–239. https://doi.org/10.1007/s10584-011-0192-8

Barnes, E. A., & Polvani, L. M. (2015). CMIP5 projections of Arctic amplification, of the North American/North Atlantic circulation, and of their relationship. *Journal of Climate*, *28*, 5254–5271. https://doi.org/10.1175/JCLI-D-14-00589.1

Barnes, E. A., & Screen, J. A. (2015). The impact of Arctic warming on the midlatitude jet stream: Can it? Has it? Will it? *Wiley Interdisciplinary Reviews: Climate Change*, *6*(3), 277–286. https://doi.org/10.1002/wcc.337

Blackport, R., & Kushner, P. J. (2018). The role of extratropical ocean warming in the coupled climate response to Arctic sea ice loss. *Journal of Climate*, *31*(22), 9193–9206. https://doi.org/10.1175/JCLI-D-18-0192.1

Blackport, R., & Screen, J. A. (2019). Influence of Arctic sea ice loss in autumn compared to that in winter on the atmospheric circulation. *Geophysical Research Letters*, *46*, 2213–2221. https://doi.org/10.1029/2018GL081469

Blackport, R., & Screen, J. A. (2020). Insignificant effect of Arctic amplification on the amplitude of midlatitude atmospheric waves. *Science Advances*, *6*(8), eaay2880. https://doi.org/10.1126/sciadv.aay2880

Blackport, R., Screen, J. A., van der Wiel, K., & Bintanja, R. (2019). Minimal influence of reduced Arctic sea ice on coincident cold winters in mid-latitudes. *Nature Climate Change 2019*, *9*, 697–704. https://doi.org/10.1038/s41558-019-0551-4

Cohen, J., Zhang, X., Francis, J., Jung, T., Kwok, R., Overland, J., & Yoon, J. (2020). Divergent consensuses on Arctic amplification influence on midlatitude severe winter weather. *Nature Climate Change*, *10*, 20–29. https://doi.org/10.1038/s41558-019-0662-y

Dai, A., Luo, D., Song, M., & Liu, J. (2019). Arctic amplification is caused by sea-ice loss under increasing CO_2. *Nature Communications*, *10*(1), 1–13. https://doi.org/10.1038/s41467-018-07954-9

Deser, C., Tomas, R., Alexander, M., & Lawrence, D. (2010). The seasonal atmospheric response to projected arctic sea ice loss in the late twenty-first century. *Journal of Climate*, *23*(2), 333–351. https://doi.org/10.1175/2009JCLI3053.1

Deser, C., Tomas, R. A., & Sun, L. (2015). The role of ocean-atmosphere coupling in the zonal-mean atmospheric response to Arctic sea ice loss. *Journal of Climate*, *28*, 2168–2186. https://doi.org/10.1175/JCLI-D-14-00325.1

Francis, J. A. (2017). Why are Arctic linkages to extreme weather still up in the air? *Bulletin of the American Meteorological Society*, *98*(12), 2551–2557. https://doi.org/10.1175/BAMS-D-17-0006.1

Francis, J. A., & Vavrus, S. J. (2015). Evidence for a wavier jet stream in response to rapid Arctic warming. *Environmental Research Letters*, *10*(1), 014,005. https://doi.org/10.1088/1748-9326/10/1/014005

Gelaro, R., McCarty, W., Suárez, M. J., Todling, R., Molod, A., Takacs, L., & Zhao, B. (2017). The modern-era retrospective analysis for research and applications, version 2 (MERRA-2). *Journal of Climate*, *30*(14), 5419–5454. https://doi.org/10.1175/JCLI-D-16-0758.1

Golaz, J. C., Caldwell, P. M., Van Roekel, L. P., Petersen, M. R., Tang, Q., Wolfe, J. D., & Zhu, Q. (2019). The DOE E3SM coupled model version 1: Overview and evaluation at standard resolution. *Journal of Advances in Modeling Earth Systems*, *11*, 2089–2129. https://doi.org/10.1029/2018MS001603

Goosse, H., Kay, J. E., Armour, K. C., Bodas-Salcedo, A., Chepfer, H., Docquier, D., & Vancoppenolle, M. (2018). Quantifying climate feedbacks in polar regions. *Nature Communications*, *9*(1), 1919. https://doi.org/10.1038/s41467-018-04173-0

Graversen, R. G., Mauritsen, T., Tjernström, M., Källén, E., & Svensson, G. (2008). Vertical structure of recent Arctic warming. *Nature*, *451*(7174), 53–56. https://doi.org/10.1038/nature06502

Hall, A., Cox, P., Huntingford, C., & Klein, S. (2019). Progressing emergent constraints on future climate change. *Nature Climate Change*, *9*(4), 269–278. https://doi.org/10.1038/s41558-019-0436-6

He, S., Xu, X., Furevik, T., & Gao, Y. (2020). Eurasia cooling linked to the vertical distribution of Arctic warming. *Geophysical Research Letters*, *47*, e2020GL087212. https://doi.org/10.1029/2020gl087212

Hersbach, H., Bell, B., Berrisford, P., Hirahara, S., Horányi, A., Muñoz-Sabater, J., & Thépaut, J. N. (2020). The ERA5 global reanalysis. *Quarterly Journal of the Royal Meteorological Society*, *146*, 1999–2049. https://doi.org/10.1002/qj.3803

Honda, M., Inoue, J., & Yamane, S. (2009). Influence of low Arctic sea-ice minima on anomalously cold Eurasian winters. *Geophysical Research Letters*, *36*, L08707. https://doi.org/10.1029/2008GL037079

Kalnay, E., Kanamitsu, M., Kistler, R., Collins, W., Deaven, D., Gandin, L., & Joseph, D. (1996). The NCEP/NCAR 40-year reanalysis project. *Bulletin of the American Meteorological Society*, *77*(3), 437–471. https://doi.org/10.1175/1520-0477(1996)077<0437:TNYRP>2.0.CO;2

Kay, J. E., Deser, C., Phillips, A., Mai, A., Hannay, C., Strand, G., & Vertenstein, M. (2015). The Community Earth System Model (CESM) large ensemble project: A community resource for studying climate change in the presence of internal climate variability. *Bulletin of the American Meteorological Society*, *96*(8), 1333–1349. https://doi.org/10.1175/BAMS-D-13-00255.1

Kim, B. M., Son, S. W., Min, S. K., Jeong, J. H., Kim, S. J., Zhang, X., & Yoon, J. H. (2014). Weakening of the stratospheric polar vortex by Arctic sea-ice loss. *Nature Communications*, *5*, 4646. https://doi.org/10.1038/ncomms5646

Labe, Z., Peings, Y., & Magnusdottir, G. (2018). Contributions of ice thickness to the atmospheric response from projected Arctic sea ice loss. *Geophysical Research Letters*, *45*, 5635–5642. https://doi.org/10.1029/2018GL078158

Labe, Z., Peings, Y., & Magnusdottir, G. (2019). The effect of QBO phase on the atmospheric response to projected Arctic sea ice loss in early winter. *Geophysical Research Letters*, *46*, 7663–7671. https://doi.org/10.1029/2019GL083095

Marsh, D. R., Mills, M. J., Kinnison, D. E., Lamarque, J. F., Calvo, N., & Polvani, L. M. (2013). Climate change from 1850 to 2005 simulated in CESM1(WACCM). *Journal of Climate*, *26*(19), 7372–7391. https://doi.org/10.1175/JCLI-D-12-00558.1

McCusker, K. E., Fyfe, J. C., & Sigmond, M. (2016). Twenty-five winters of unexpected Eurasian cooling unlikely due to Arctic sea-ice loss. *Nature Geoscience*, *9*(11), 838–842. https://doi.org/10.1038/ngeo2820

Mori, M., Kosaka, Y., Watanabe, M., Nakamura, H., & Kimoto, M. (2019). A reconciled estimate of the influence of Arctic sea-ice loss on recent Eurasian cooling. *Nature Climate Change*, *9*, 123–129. https://doi.org/10.1038/s41558-018-0379-3

Mori, M., Watanabe, M., Shiogama, H., Inoue, J., & Kimoto, M. (2014). Robust Arctic sea-ice influence on the frequent Eurasian cold winters in past decades. *Nature Geoscience*, *7*(12), 869–873. https://doi.org/10.1038/ngeo2277

Nakamura, T., Yamazaki, K., Honda, M., Ukita, J., Jaiser, R., Handorf, D., & Dethloff, K. (2016). On the atmospheric response experiment to a Blue Arctic Ocean. *Geophysical Research Letters*, *43*, 10,394–10,402. https://doi.org/10.1002/2016GL070526

Nakamura, T., Yamazaki, K., Iwamoto, K., Honda, M., Miyoshi, Y., Ogawa, Y., & Ukita, J. (2015). A negative phase shift of the winter AO/NAO due to the recent Arctic sea-ice reduction in late autumn. *Journal of Geophysical Research: Atmospheres*, *120*, 3209–3227. https://doi.org/10.1002/2014JD022848

Ogawa, F., Keenlyside, N., Gao, Y., Koenigk, T., Yang, S., Suo, L., & Semenov, V. (2018). Evaluating impacts of recent Arctic sea-ice loss on the Northern Hemisphere winter climate change. *Geophysical Research Letters*, *45*, 3255–3263. https://doi.org/10.1002/2017GL076502

Panagiotopoulos, F., Shahgedanova, M., Hannachi, A., & Stephenson, D. B. (2005). Observed trends and teleconnections of the Siberian High: A recently declining center of action. *Journal of Climate*, *18*(9), 1411–1422. https://doi.org/10.1175/JCLI3352.1

Park, K., Kang, S. M., Kim, D., Stuecker, M. F., & Jin, F. F. (2018). Contrasting local and remote impacts of surface heating on polar warming and amplification. *Journal of Climate*, *31*(8), 3155–3166. https://doi.org/10.1175/JCLI-D-17-0600.1

Peings, Y. (2019). Ural blocking as a driver of early-winter stratospheric warmings. *Geophysical Research Letters*, *46*, 5460–5468. https://doi.org/10.1029/2019GL082097

Peings, Y., Cattiaux, J., & Magnusdottir, G. (2019). The Polar Stratosphere as an arbiter of the Projected Tropical Versus Polar Tug of War. *Geophysical Research Letters*, *46*, 9261–9270. https://doi.org/10.1029/2019GL082463

Peings, Y., Cattiaux, J., Vavrus, S. J., & Magnusdottir, G. (2018). Projected squeezing of the wintertime North-Atlantic jet. *Environmental Research Letters*, *13*, 074,016. https://doi.org/10.1088/1748-9326/aacc79

Peings, Y., & Magnusdottir, G. (2014). Response of the wintertime Northern Hemisphere atmospheric circulation to current and projected Arctic sea ice decline: A numerical study with CAM55. *Journal of Climate*, *27*(1), 244–264. https://doi.org/10.1175/JCLI-D-13-00272.1

Perlwitz, J., Hoerling, M., & Dole, R. (2015). Arctic tropospheric warming: Causes and linkages to lower latitudes. *Journal of Climate*, *28*(6), 2154–2167. https://doi.org/10.1175/JCLI-D-14-00095.1

Rasch, P. J., Xie, S., Ma, P. L., Lin, W., Wang, H., Tang, Q., & Yang, Y. (2019). An overview of the atmospheric component of the Energy Exascale Earth System Model. *Journal of Advances in Modeling Earth Systems*, *11*, 2377–2411. https://doi.org/10.1029/2019MS001629

Rayner, N. A., Parker, D. E., Horton, E. B., Folland, C. K., Alexander, L. V., Rowell, D. P., & Kaplan, A. (2003). Global analyses of sea surface temperature, sea ice, and night marine air temperature since the late nineteenth century. *Journal of Geophysical Research*, *108*(D14), 4407. https://doi.org/10.1029/2002JD002670

Richter, J. H., Chen, C., Tang, Q., Xie, S., & Rasch, P. J. (2019). Improved simulation of the QBO in E3SMv1. *Journal of Advances in Modeling Earth Systems*, *11*, 3403–3418. https://doi.org/10.1029/2019MS001763

Santer, B. D., Fyfe, J. C., Pallotta, G., Flato, G. M., Meehl, G. A., England, M. H., & Zou, C. Z. (2017). Causes of differences in model and satellite tropospheric warming rates. *Nature Geoscience*, *10*(7), 478–485. https://doi.org/10.1038/ngeo2973

Schweiger, A., Lindsay, R., Zhang, J., Steele, M., Stern, H., & Kwok, R. (2011). Uncertainty in modeled Arctic sea ice volume. *Journal of Geophysical Research*, *116*, C00D06. https://doi.org/10.1029/2011JC007084

Screen, J. A., Deser, C., & Simmonds, I. (2012). Local and remote controls on observed Arctic warming. *Geophysical Research Letters*, *39*, L10709. https://doi.org/10.1029/2012GL051598

Screen, J. A., Deser, C., & Sun, L. (2015). Reduced risk of North American cold extremes due to continued Arctic sea ice loss. *Bulletin of the American Meteorological Society*, *96*(9), 1489–1503. https://doi.org/10.1175/BAMS-D-14-00185.1

Screen, J. A., & Simmonds, I. (2011). Erroneous Arctic temperature trends in the ERA-40 reanalysis: A closer look. *Journal of Climate*, *24*(10), 2620–2627. https://doi.org/10.1175/2010JCLI4054.1

Screen, J. A., Simmonds, I., Deser, C., & Tomas, R. (2013). The atmospheric response to three decades of observed Arctic sea ice loss. *Journal of Climate*, *26*(4), 1230–1248. https://doi.org/10.1175/JCLI-D-12-00063.1

Sellevold, R., Sobolowski, S., & Li, C. (2016). Investigating possible Arctic-Midlatitude teleconnections in a linear framework. *Journal of Climate*, *29*(20), 7329–7343. https://doi.org/10.1175/JCLI-D-15-0902.1

Smith, K. L., Neely, R. R., Marsh, D. R., & Polvani, L. M. (2014). The specified chemistry whole atmosphere community climate model (SC-WACCM). *Journal of Advances in Modeling Earth Systems*, *6*, 883–901. https://doi.org/10.1002/2014MS000346

Smith, D. M., Screen, J. A., Deser, C., Cohen, J., Fyfe, J. C., García-Serrano, J., & Zhang, X. (2019). The Polar Amplification Model Intercomparison Project (PAMIP) contribution to CMIP6: Investigating the causes and consequences of polar amplification. *Geoscientific Model Development*, *12*(3), 1139–1164. https://doi.org/10.5194/gmd-12-1139-2019

Stuecker, M. F., Bitz, C. M., Armour, K. C., Proistosescu, C., Kang, S. M., Xie, S. P., & Jin, F. F. (2018). Polar amplification dominated by local forcing and feedbacks. *Nature Climate Change*, *8*(12), 1076–1081. https://doi.org/10.1038/s41558-018-0339-y

Sun, L., Deser, C., & Tomas, R. A. (2015). Mechanisms of stratospheric and tropospheric circulation response to projected Arctic sea ice loss. *Journal of Climate*, *28*, 7824–7845. https://doi.org/10.1175/JCLI-D-15-0169.1

Taylor, K. E., Williamson, D. L., & Zwiers, F. W. (2000). The sea surface temperature and sea-ice concentration boundary conditions for AMIP II simulations. *PCMDI Report Series*, *60*, 28.

Thompson, D. W. J., & Wallace, J. M. (1998). The Arctic oscillation signature in the wintertime geopotential height and temperature fields. *Geophysical Research Letters*, *25*(9), 1297–1300. https://doi.org/10.1029/98GL00950

Thyng, K., Greene, C., Hetland, R., Zimmerle, H., & DiMarco, S. (2016). True colors of oceanography: Guidelines for effective and accurate colormap selection. *Oceanography*, *29*(3), 9–13. https://doi.org/10.5670/oceanog.2016.66

Vavrus, S. J. (2018). The influence of Arctic amplification on mid-latitude weather and climate. *Current Climate Change Reports*, *4*(3), 238–249. https://doi.org/10.1007/s40641-018-0105-2

Wilks, D. S. (2016). "The stippling shows statistically significant grid points": How research results are routinely overstated and overinterpreted, and what to do about it. *Bulletin of the American Meteorological Society*, *97*(12), 2263–2273. https://doi.org/10.1175/BAMS-D-15-00267.1

Xu, X., He, S., Gao, Y., Furevik, T., Wang, H., Li, F., & Ogawa, F. (2019). Strengthened linkage between midlatitudes and Arctic in boreal winter. *Climate Dynamics*, *53*(7-8), 3971–3983. https://doi.org/10.1007/s00382-019-04764-7

Zappa, G., Pithan, F., & Shepherd, T. G. (2018). Multi-model evidence for an atmospheric circulation response to Arctic sea ice loss in the CMIP5 future projections. *Geophysical Research Letters*, *45*, 1011–1019. https://doi.org/10.1002/2017GL076096

Zhang, P., Wu, Y., Simpson, I. R., Smith, K. L., Zhang, X., De, B., & Callaghan, P. (2018). A stratospheric pathway linking a colder Siberia to Barents-Kara Sea sea ice loss. *Science Advances*, *4*(7), eaat6025. https://doi.org/10.1126/sciadv.aat6025